LA-UR-21-25645
Approved for public release; distribution is unlimited.

Title:	Reference document for LANL stack sampling and ANSI N13.1 (Article) Gielow RL and McNamee MR 1993. Numerical Flue Gas Flow Modeling for Continuous Emissions Monitoring Applications. EPRI CEM Users Group Meeting. Baltimore. RP1961-13.
Author(s):	Moore, Murray E. Glissmeyer, John A. Barnett, J. Matthew
Intended for:	Provide archive access for a reference for technical standard ANSI N13.1 (2011). Report
Issued:	2021-06-16 (rev.1)

LA-UR-21-25645
Approved for public release; distribution is unlimited.

Title: Reference document for LANL stack sampling and ANSI N13.1 (Article) Gielow RL and McNamee MR 1993. Numerical Flue Gas Flow Modeling for Continuous Emissions Monitoring Applications. EPRI CEM Users Group Meeting. Baltimore. RP1961-13.

Author(s): Moore, Murray E.
Glissmeyer, John A.
Barnett, J. Matthew

Intended for: Provide archive access for a reference for technical standard ANSI N13.1 (2011).
Report

Issued: 2021-06-15

Murray E. Moore
Los Alamos National Laboratory

John A. Glissmeyer
Glissmeyer Environmental, LLC

J. Matthew Barnett
Pacific Northwest National Laboratory

June 2021

Reference document for LANL stack sampling and ANSI N13.1 (Article) Gielow RL and McNamee MR 1993. Numerical Flue Gas Flow Modeling for Continuous Emissions Monitoring Applications. EPRI CEM Users Group Meeting. Baltimore. RP1961-13.

INTRODUCTION

American National Standard N13.1 "sets forth guidelines and performance criteria for sampling the emissions of airborne radioactive substances in the air discharge ducts and stacks of nuclear facilities. Emphasis is on extractive sampling from a location in a stack or duct where the contaminant is well mixed. At such a location, sampling may be conducted at a single point. This standard provides performance-based criteria for the use of air sampling probes, transport lines, sample collectors, sample monitoring instruments, and gas flow measuring methods. This standard also covers sampling program objectives, quality assurance issues, developing air sampling action levels, system optimization, and system performance verification. Workplace, containment, and environmental air monitoring are not addressed. Specific sample analysis methods and the reporting or interpreting of results are also not addressed." (HPS 2011).

RATIONALE

This 2021 document is intended to provide electronic archive access for a publication (Gielow and McNamee 1993) that is referenced in the ANSI N13.1 standard (HPS 2011). Note the technical standard ANSI N13.1 is a dual publication by ANSI and by the Health Physics Society.

In the course of document review, it was observed that the Gielow and McNamee article was not available on the Internet for electronic access. Multiple persons on the ANSI N13.1 writing committee searched in vain for the article.

However, Robert Mudry of the Airflow Sciences Corporation (Livonia, MI) was able to find the article in their hardcopy archives. (RL Gielow is the founder of the Airflow Sciences company, and his firm performed the original work.)

REFERENCES

Gielow, R.L.; McNamee, M.R. Numerical Flue Gas Flow Monitoring for Continuous Emissions Monitoring Applications. Presented at the CEM Users Group Meeting, sponsored by the Electric Power Research Institute, held in Baltimore, Maryland, April 13-15; 1993.

HPS. 2011. Sampling and Monitoring Releases of Airborne Radioactive Substances from the Stacks and Ducts of Nuclear Facilities. ANSI/HPS N13.1-2011. Health Physics Society. McLean, VA.

ATTACHMENT

Gielow and McNamee (1993) article

Numerical Flue Gas Flow Modeling for Continuous Emissions Monitoring Applications

by

Airflow Sciences Corporation

Prepared for:

Electric Power Research Institute (EPRI)

RP1961-13: Guidelines for Flue Gas Flow Rate Monitoring

Presented at the

CEM Users Group Meeting

Sponsored by
Electric Power Research Institute
and
Baltimore Gas and Electric Company

April 13-15, 1993
Baltimore, Maryland

R. L. Gielow

M. R. McNamee

Airflow Sciences Corporation
37453 Schoolcraft Rd
Livonia, MI 48150-1007

Numerical Flue Gas Flow Modeling for Continuous Emissions Monitoring Applications

Numerical flow models of three CEM sites are to be developed in conjunction with an Electric Power Research Institute (EPRI) project entitled "Guidelines for Flue Gas Flow Rate Monitoring". The computational approach, which evolved from the aerospace industry's endeavors into the field of computational fluid dynamics (CFD), provides a wealth of information and options that would be very difficult to achieve through testing or cold flow physical modeling alone. The first of the three models, simulating the flow of hot flue gas in the breeching ductwork at Ohio Edison's Edgewater Station, has been completed. This paper presents the results of the numerical simulation, a comparison with actual test measurements, and possible uses relating to CEM applications.

I. INTRODUCTION

This paper contains the results of the first of three flow models to be developed for the "Guidelines for Flue Gas Flow Rate Monitoring" project being sponsored by the Electric Power Research Institute (EPRI). The model simulates the flow of flue gas through the breeching ductwork of Ohio Edison's Edgewater Station. The goal of the numerical modeling effort is to show that computational fluid dynamics may be used to help utilities optimize the placement, testing, and calibration of continuous emissions monitoring devices within a duct leading to the stack.

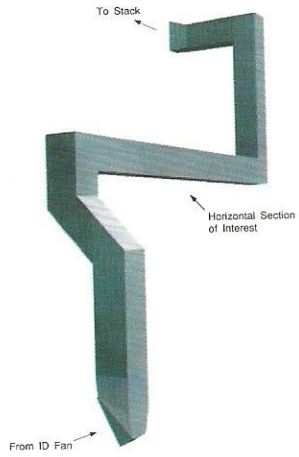

Figure 1. Simplified view of the ductwork.

Edgewater Station Model

The ductwork leading from the ID fan to the stack at Ohio Edison's Edgewater Station, Unit 4, was chosen as the first configuration to be modeled. A simplified display of the section of ductwork modeled is shown in Figure 1. The primary section of interest, the 115 ft long horizontal portion, is connected at the upstream end to a dog-leg duct rising 60 ft from the exit of the ID fan. Downstream of the horizontal section, the ductwork rises another 50 feet before turning toward the stack (located 30 feet to the side). Both the entrance and exit of the horizontal duct terminate at 90 degree elbows.

II. APPROACH

The flow of hot flue gas within the ductwork was modeled using an in-house CFD package known as **VISCOUS**. The program is based on a control volume approach which states that a domain may be divided into a number of non-overlapping sub-domains, or control volumes. The governing equations for conservation of mass, momentum, energy, and chemical species are then integrated in a piece-wise fashion over each of the control volumes. This insures that the conservation equations are satisfied over each "cell" used to represent the geometry. The integration procedure results in a set of discretized equations for each control volume which can then be solved by a computer.

In order to model the three-dimensional nature of the Edgewater Station ductwork with the required amount of detail, a technique has been developed which allows large domains to be broken up into smaller, more manageable

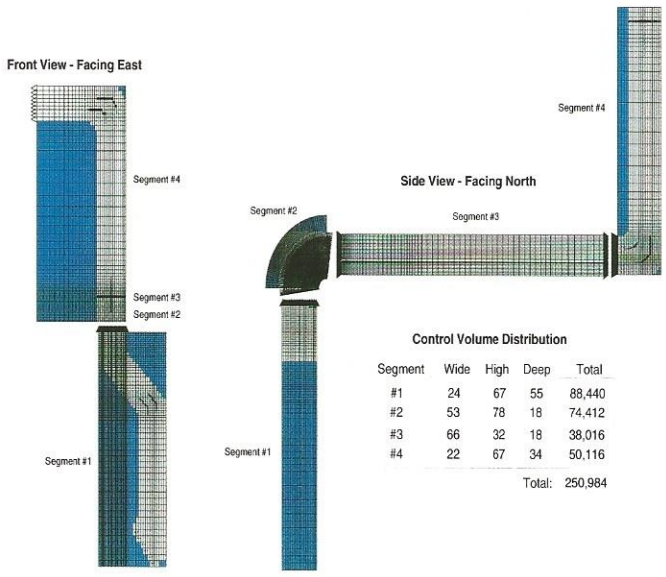

Figure 2. Schematic of segmented computational domain.

segments. Each segment is then allowed to communicate with adjoining segments to ensure that the correct overall flow field is achieved.

As shown in Figure 2, the Edgewater Station ductwork has been sub-divided into the following four segments (or computational domains):

1. The dog-leg section running from the ID fan to the first 90 degree elbow.
2. The first 90 degree elbow.
3. The horizontal section between the first and second 90 degree elbows.
4. The remaining sections, including the second and third 90 degree elbows and the exit to the stack.

Although this segmenting technique substantially reduces the number of cells (or control volumes) required, the final models still total approximately 250,000 cells as tabulated in Figure 2.

Simulated Flow Rates

Computer simulations were performed for three different flow rates in order to investigate the sensitivity of the flow profile to changes in flow volume. The following flow rates were used for the three different cases:

1. Low flow rate: 167,000 acfm @ 250 °F
2. Medium flow rate: 275,000 acfm @ 273 °F
3. High flow rate: 429,500 acfm @ 296 °F

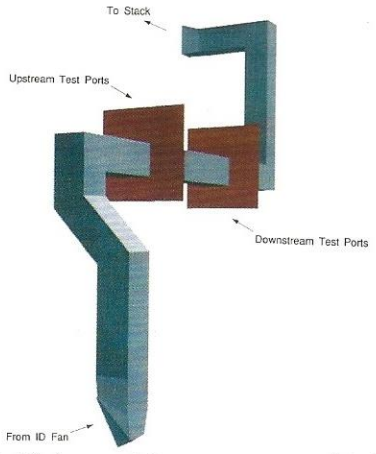

Figure 3. Upstream and downstream test port locations.

Experimental Test Conditions

The Edgewater Station was chosen for the initial phase of this study because of the quantity and quality of the test data available from this site. Ohio Edison had installed test ports at two locations and tested several different continuous emissions monitoring devices within the breeching ductwork. Velocity traverses had been conducted using both s-type pitot tubes and a 3-D probe. As shown in Figure 3, the first plane in which test ports are located is approximately 28 feet downstream from the Segment #2 turn and is identified as the "upstream" location. Other test ports are positioned in a plane located 86 feet downstream from the turn that is identified as the "downstream" location. Test measurements were taken at these locations during November of 1991 and again during February, March, and May of 1992. A 5 by 8 matrix of measurement points was used for the 3-D probe velocity traverses (see Figure 4) and a similar 5 by 5 matrix was used for the pitot tube tests.

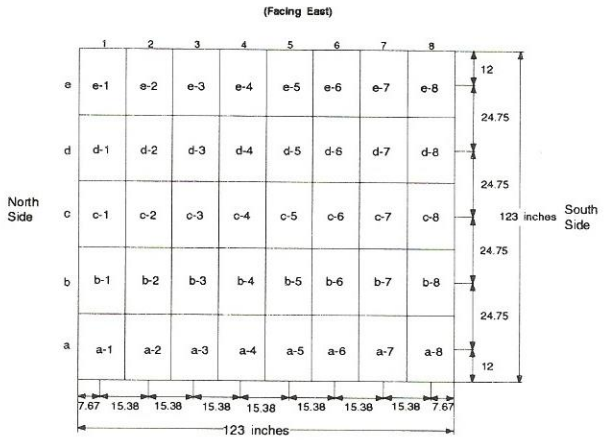

Figure 4. Test traverse points for 3-D measurements.

III. RESULTS

Simulated Flow Field Results

Figures 5 through 9 show color contours of predicted velocity distributions within the duct. These results were obtained for the high flow rate case. However, similar flow field characteristics were noted in each of the reduced flow rate simulations. Figure 5 depicts the flow field through the dog-leg section, Segment #1, originating at the ID fan. Higher gas velocities are noted along the outer (right side) wall. This leads to higher speed flow through the outside of the first 45 degree turn and the inside of the second turn.

A cross-section of the flow field in the upstream 90 degree elbow (Segment #2) is illustrated in Figure 6. This contour plot shows that higher speed flow follows a path which stays to the inside of the turn. A comparison of this plot with Figure 5 suggests that the flow distribution entering the turn is non-uniform in both directions.

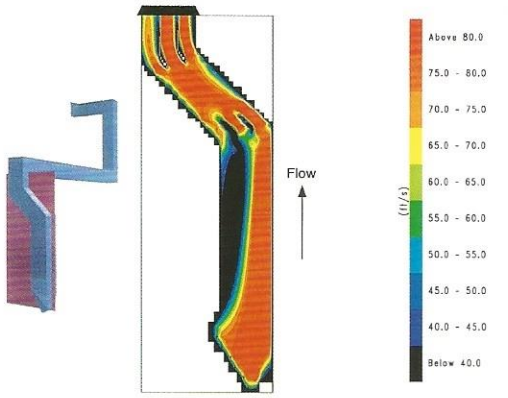

Figure 5. Velocity contours in the indicated plane (front view) of Segment #1, the dog-leg section.

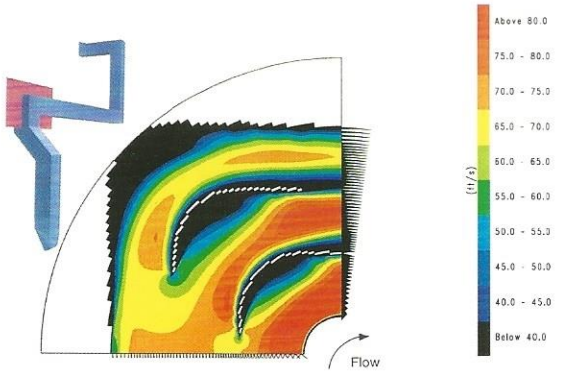

Figure 6. Velocity contours in the indicated plane (side view) of Segment #2, the upstream elbow.

Figure 7 shows the flow distribution along the length of the horizontal duct, Segment #3. Figure 7 clearly shows that flow entering this segment has a sizeable upward component. The following section of this report contains additional discussions regarding the flow in this segment, which contains the test port planes.

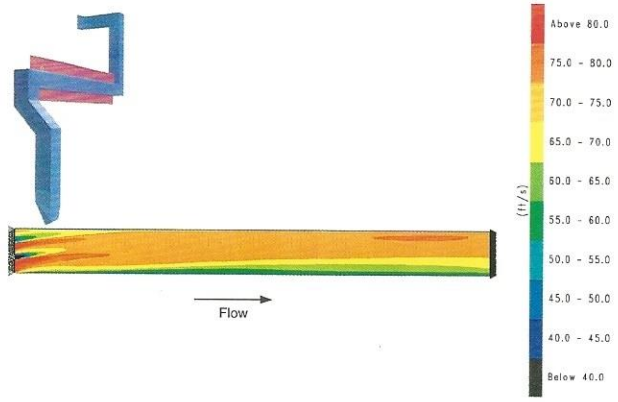

Figure 7. Velocity contours in the indicated plane (side view) of Segment #3, the horizontal duct.

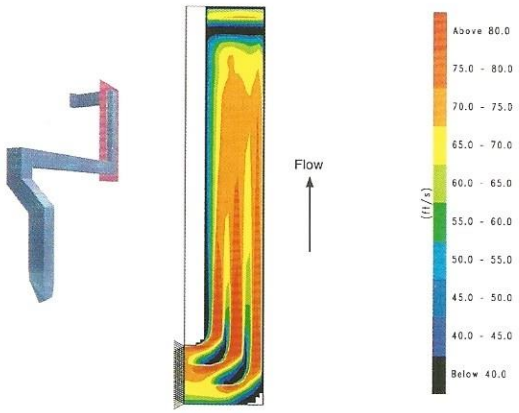

Figure 8. Velocity contours in the indicated plane (side view) of Segment #4, the section leading to the stack.

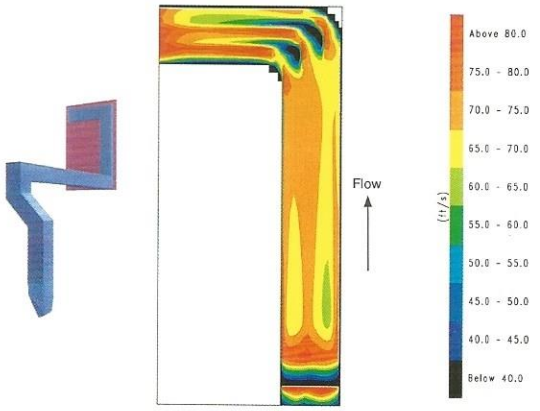

Figure 9. Velocity contours in the indicated plane (front view) of Segment #4, the section leading to the stack.

Figures 8 and 9 show the flow distribution in Segment #3. Once again, the flow field tends to be non-uniform for most of the straight duct sections, although it diffuses somewhat over the lengths of the ducts.

Velocity Field in the Horizontal Duct, Segment #3

Because the test ports are located in planes normal to the horizontal duct section, it is Segment #3 which is of paramount interest in this study. Figures 10 through 12 show color-coded speed profiles and velocity components at four different locations: the upstream end of the duct, the upstream test port location, the downstream test port location, and the downstream end of the duct. Figure 10 shows the flow profiles for the high flow rate case, Figure 11 illustrates the profiles for the medium flow rate case, and Figure 12 shows the low flow rate profiles. Comparing each of the three sets and noting the changes in scale, it is evident that flow distribution is relatively insensitive to changes in flow rate. In other words, the magnitudes of the velocities are scaled nearly proportionally. The upstream end sections show that the flow field is highly non-uniform at the entrance

to the horizontal duct. In fact, it contains at least three different vortex pairs and a velocity profile that is skewed towards the bottom of the duct.

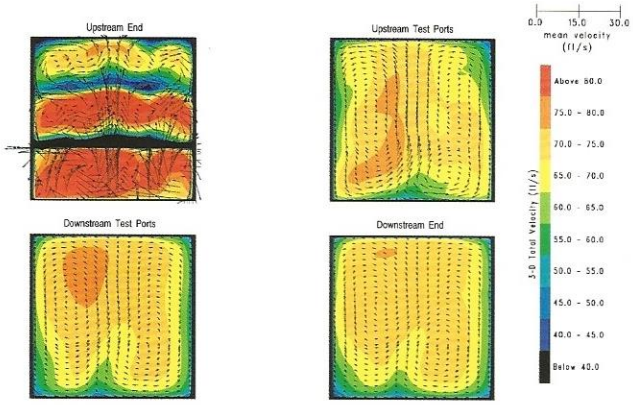

Figure 10. Velocity contours at four stations along the horizontal duct, high flow rate case.

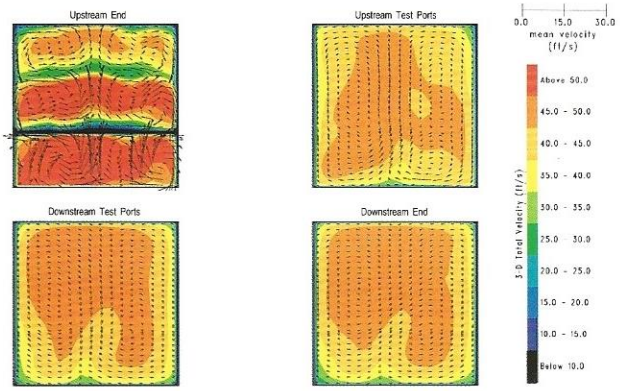

Figure 11. Velocity contours at four stations along the horizontal duct, medium flow rate case.

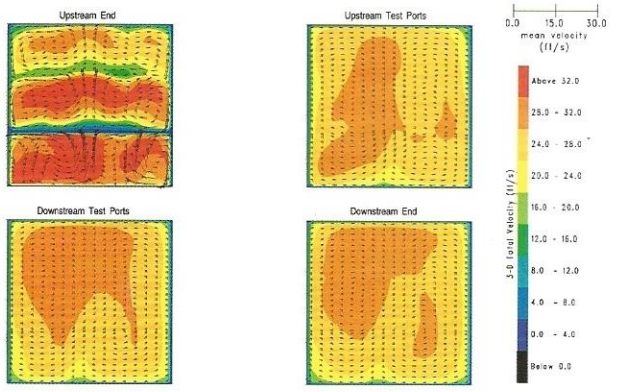

Figure 12. Velocity contours at four stations along the horizontal duct, low flow rate case.

The upstream test port locations show that total velocities lie in the range from 55 to 80 ft/sec for the high flow rate, 35 to 50 ft/sec for the medium flow rate, and 20 to 32 ft/sec for the low flow rate cases. At this location, the multiple vortex pairs that were visible at the upstream entrance to the duct have merged into a single, counter-rotating vortex pair. The downstream test port locations show a similar flow field to that of the upstream locations. However, the velocity gradients have diminished and the higher velocity core has moved to the upper, left hand quadrant of the duct. At the downstream end of the duct, the total velocity plots are similar to those at the downstream port locations, with a slightly more diffused flow field.

Resultant Angles in the Horizontal Duct Section

Ohio Edison performed 3-D probe tests in order to measure the angularity of the flow at each of the two test port locations. In computing the numerical field, program **VISCOUS** provides all of the information necessary to calculate the flow angles at any point in the field. Figures 13 through 15 show plots of the resultant angles, given in units of degrees, for each of the flow rates at the same four locations defined earlier for Figures 10 through 12. Figure 13 shows the flow angularity for the high flow rate case while Figure

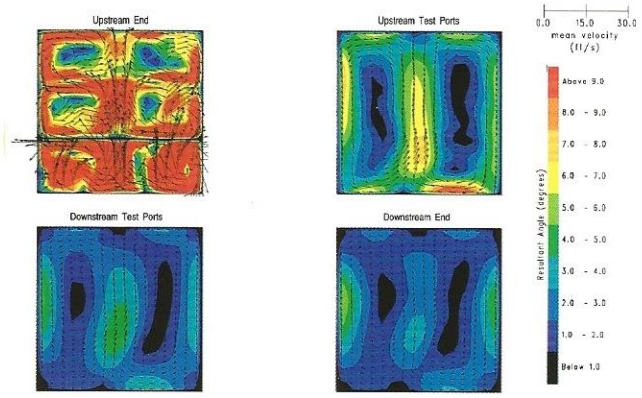

Figure 13. Resultant angle contours at four stations along the horizontal duct, high flow rate case.

14 shows the same information for the medium flow rate case. Finally, Figure 15 displays the angles for the low flow rate case. These plots illustrate that the resultant angles relative to the flow direction are in the 0 to 9 degree range at the upstream location and in the 0 to 5 degree range for the downstream location. The counter rotating vortices, which are normally found downstream of a bend in a duct, are clearly visible and are primarily responsible for the resultant flow angularity.

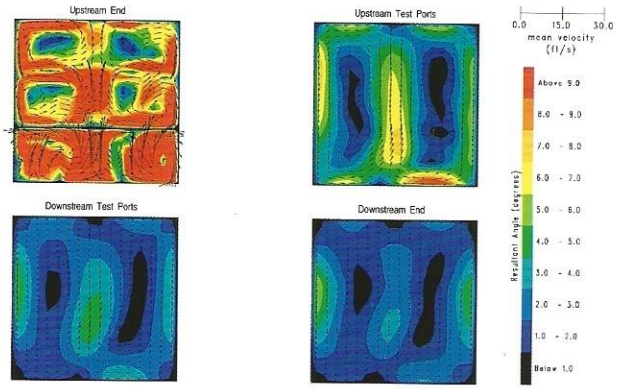

Figure 14. Resultant angle contours at four stations along the horizontal duct, medium flow rate case.

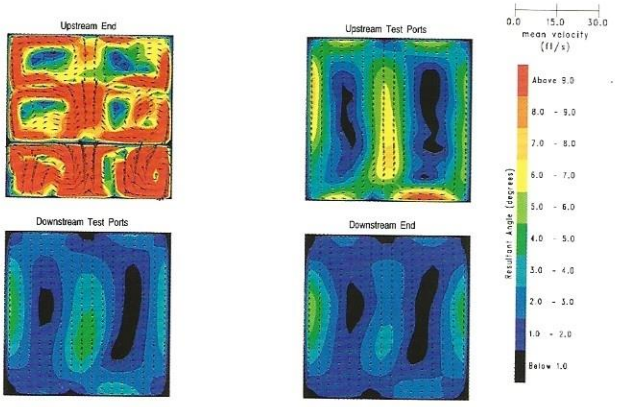

Figure 15. Resultant angle contours at four stations along the horizontal duct, low flow rate case.

Simulated Flow Monitor Output

The numerical model can be used to predict the output from a flow monitor placed within a duct at a particular location. The simulated results include the effects of flow stratification, vorticity, and thermal gradients at the particular site. Thus, the model can be used to aid in the selection of flow monitor placement.

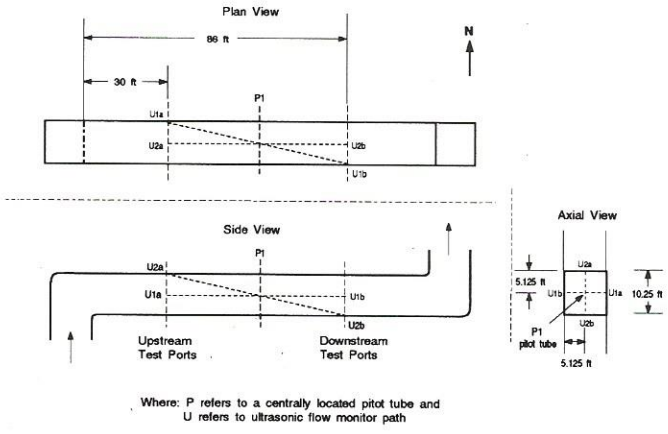

Figure 16. Schematic of simulated flow monitor placement.

As an example, a comparison is made between the simulated output from three generic flow monitors placed in the Edgewater Station model. The three cases are as follows (see Figure 16):

1. An ultrasonic flow monitor with its upstream transducer located in the center of the north wall at the upstream test port location (U1a). The downstream test port location (U1b) houses the downstream transducer in the center of the south wall.

2. An ultrasonic flow monitor placed with its upstream transducer located on the roof of the duct at the upstream test port position (U2a). The downstream transducer (U2b) is positioned on the floor of the duct at the downstream test port location.

3. A pitot tube (P1) centrally located halfway between the two test port locations.

Simulated flow monitor output is normalized by the average velocity in the duct. Results for the three cases were obtained by extracting the appropriate velocity data from the simulated flow fields. As shown in Figure 17, both types of flow monitors display little sensitivity to flow rate fluctuations, however, differences can result due to placement. From this informal study, it appears that the horizontally oriented ultrasonic flow monitor produces the result with the least bias.

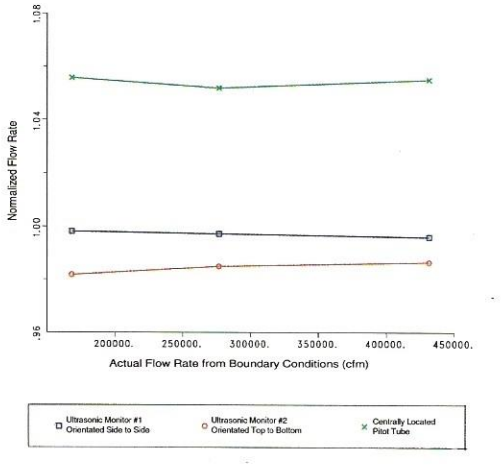

Figure 17. Numerical results from simulated monitors.

A Simulated Flow Field Modification

Besides being able to simulate the output from flow monitors for the baseline duct geometry, CFD can be used to evaluate the effects of modifications designed to improve the site's overall performance. Modifications using perforated plates, nozzles, turning vanes or the addition of flow straightening devices can be simulated, usually with a minor adjustment to the baseline model.

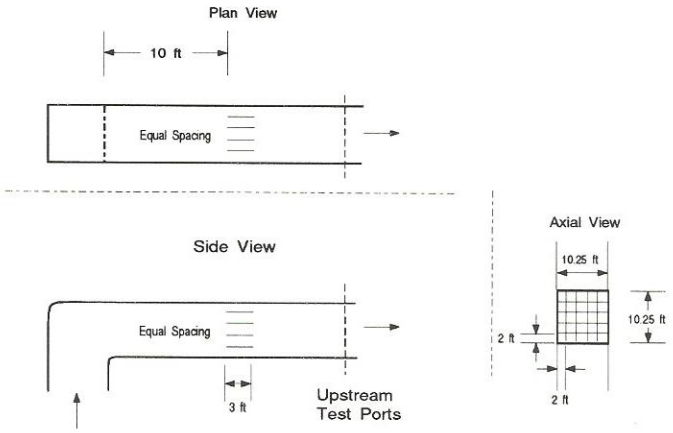

Figure 18. Details of the simulated flow straightening device.

As an example of how numerical modeling can be used to evaluate the effect of hardware modifications, a flow straightening device was inserted into the high flow rate simulation of the horizontal duct section (see Figure 18). The device simulated consists of four equally-spaced horizontal and four equally-spaced vertical plates. The plates are placed approximately 10 feet from the end of the upstream corner and extend 3 feet downstream. This "egg-crate-like" device forces the flue gas through relatively small, straight channels which effectively dissipate the side-to-side and vertical velocity components in the flue gas stream without a noticeable sacrifice in pressure. Flow straighteners can be used effectively in cases where minimal flow angularity is desired. Figures 19 and 20 show the effects of the aforementioned

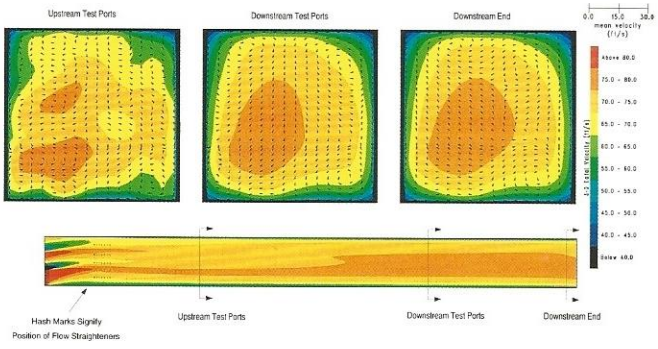

Figure 19. Effect of the flow straightener on the velocity field.

device on local velocities and angles at various downstream stations along the duct. The flow straightening device produces a smoother, more fully developed total velocity profile as is evident in Figure 19. Meanwhile, Figure 20 shows the drastic reduction of the flow angularity downstream of the straightener (note the 10-to-1 change in scale from Figure 13). In effect, the flow angles are reduced to near zero.

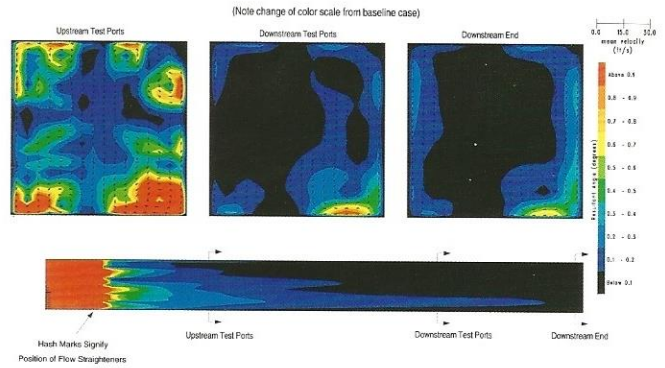

Figure 20. Effect of the straightener on the flow angularity.

IV. CONCLUSIONS

Velocity Profile Comparisons

To compare the experimental and simulated test results, both data sets are plotted on the same graph. The simulation results include a "Turbulence Band" based on the results of a turbulence model incorporated into the program **VISCOUS** flow code. The selected k-ε turbulence model is a commonly used numerical approximation for the turbulent viscosity that

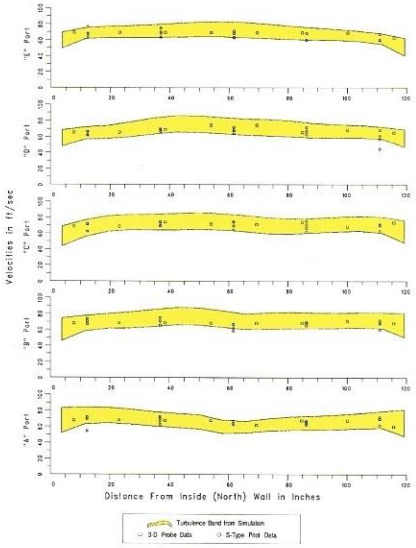

Figure 21. High flow rate velocity comparison (upstream ports).

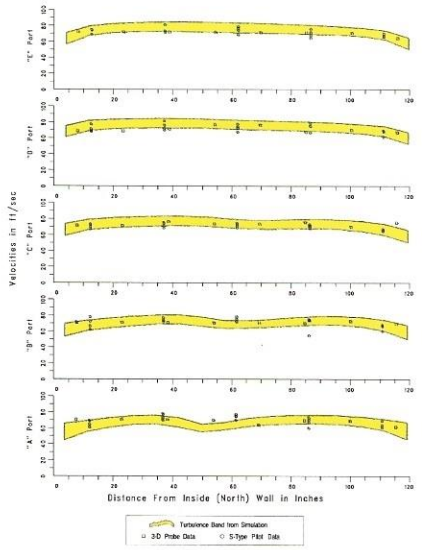

Figure 22. High flow rate velocity comparison (downstream ports).

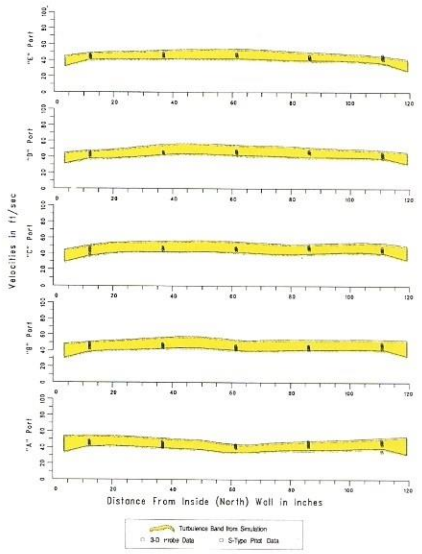

Figure 23. Medium flow rate velocity comparison (upstream ports).

produces, as a by-product of its calculations, the turbulent kinetic energy, k. The formulation for the k term is as follows:

$$k = 1/2\ (u'^2 + v'^2 + w'^2)$$

where u', v', and w' are the components of the turbulent velocity fluctuations, V'_t. The magnitude of the time-dependent fluctuation can then be found by:

$$|V'_t| = \sqrt{(2k)}$$

This value is added to and subtracted from the predicted steady-state value to describe a band identifying the turbulent range of velocities predicted by the numerical model. The readings from an ideal velocity monitor, with perfect accuracy and precision, should fall within these bands. Figures 21 through 26 show comparison plots for the simulated turbulence bands versus the experimental s-type and 3-D pitot probe data for each vertical sample location (A-E) at each test location. These plots are organized by flow rate and then upstream/downstream location. The following items can be surmised from these plots:

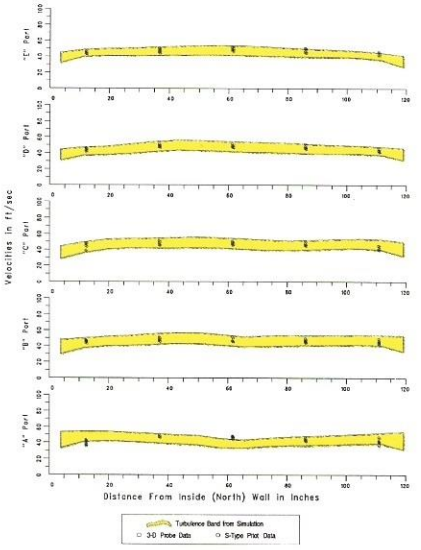

Figure 24. Medium flow rate velocity comparison (downstream ports).

- Good correlation is achieved.
- The width of the predicted turbulence band increases as the flow rate is increased.
- The scatter in the test data appears to become greater for the higher flow rate cases.

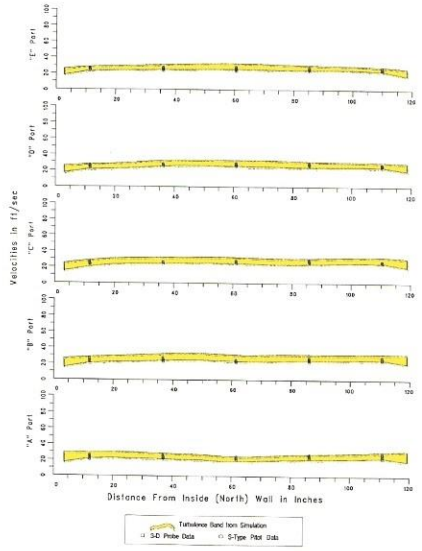

Figure 25. Low flow rate velocity comparison (upstream ports).

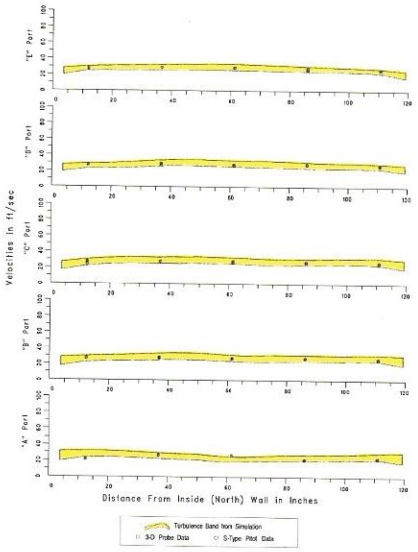

Figure 26. Low flow rate velocity comparison (downstream ports).

Resultant Angle Comparisons

As previously mentioned, Ohio Edison obtained resultant angle measurements using a 3-D pitot probe. A comparison of the flow angles reveals that nearly all of the experimental angles are between 6° and 8° for the upstream and downstream test port locations, whereas the simulated angles vary

Resultant Angles from the Numerical Model

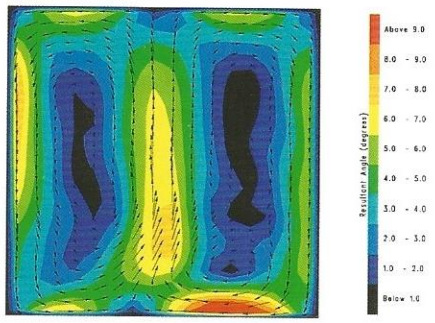

Resultant Angles from 3-D Probe Measurements in Degrees

Horizontal Position

Vertical Position	1	2	3	4	5	6	7	8
E	7.1, *.*, *.*	7.7, *.*, *.*	7.3, *.*, *.*	6.9, *.*, *.*	6.9, *.*, *.*	6.9, *.*, *.*	6.9, *.*, *.*	6.9, *.*, *.*
D	6.9, 6.9, 8.2	8.3, *.*, *.*	8.3, *.*, *.*	6.9, *.*, *.*	6.9, *.*, *.*	7.0, *.*, *.*	7.3, *.*, *.*	7.1, *.*, *.*
C	6.9, 7.3, 6.8	6.9, 6.9, 7.6	6.9, 7.3, 6.5	6.3, 7.0, 6.5	6.3, 6.9, 6.5	6.9, 6.9, 6.8	6.9, 8.9, 7.6	6.9, 7.0, 3.2
B	6.9, 7.7, 2.3	6.9, 6.9, 3.7	6.9, 6.9, 4.0	7.3, 7.8, 6.8	7.3, 8.3, 6.5	7.3, 6.9, 6.8	6.9, 7.3, 6.8	6.9, 6.9, 6.8
A	3.6, 6.9, 3.8	3.0, 6.9, 5.5	2.8, 6.9, 2.0	8.9, 7.3, 6.0	7.0, 7.3, 8.0	6.9, 7.3, 4.9	7.0, 7.3, 7.1	6.9, 7.3, 5.1

Where: Top # ==> High Flowrate - March Data 3D-UP-1
Middle # ==> Medium Flowrate - May Data 3D-UP-2
Lower # ==> Low Flowrate - February Data 3D-1-UP
and "*" indicates a missing data point

Figure 27. Upstream resultant angle comparison.

Resultant Angles from the Numerical Model

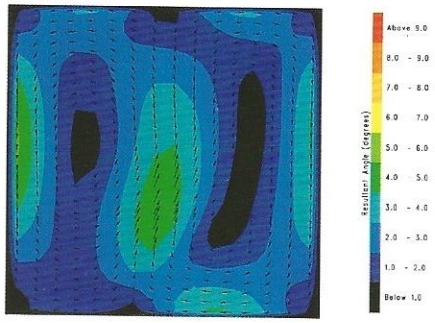

Resultant Angles from 3-D Probe Measurements in Degrees

Horizontal Position

Vertical Position	1	2	3	4	5	6	7	8
E	7.1, *.*, *.*	7.7, *.*, *.*	7.3, *.*, *.*	6.9, *.*, *.*	6.9, *.*, *.*	6.9, *.*, *.*	6.9, *.*, *.*	6.9, *.*, *.*
D	6.9, 7.3, 4.6	8.3, *.*, *.*	8.3, *.*, *.*	6.9, *.*, *.*	6.9, *.*, *.*	7.0, *.*, *.*	7.3, *.*, *.*	7.1, *.*, *.*
C	6.9, 7.7, 3.4	6.9, 6.9, 4.1	6.9, 6.9, 4.3	6.3, 6.9, 7.1	6.3, 7.1, 6.5	6.9, 7.0, 6.5	6.9, 6.9, 7.6	6.9, 7.3, 7.1
B	6.9, 7.7, 6.8	6.9, 6.9, 6.5	6.9, 6.9, 8.2	7.3, 8.3, 6.5	7.3, 7.0, 7.1	7.3, 6.9, 4.1	6.9, 6.9, 6.5	6.9, 6.9, 7.1
A	3.6, 7.0, 6.5	3.0, 7.1, 6.5	2.8, 6.9, 6.5	8.9, 6.9, 1.3	7.0, 7.1, 4.0	6.9, 7.3, 3.5	7.0, 8.2, 1.4	6.9, 8.3, 9.0

Where: Top # ==> High Flowrate - March Data 3D-DOWN-1
Middle # ==> Medium Flowrate - May Data 3D-DN-2
Lower # ==> Low Flowrate - February Data 3D-1-DOWN
and "*" indicates a missing data point

Figure 28. Downstream resultant angle comparison .

from 0° to 9° and from 0° to 5°, respectively (see Figures 27 and 28). The maximum flow angles from the simulation lie on the perimeter of the counter-rotating vortices generated by the upstream bend, with near zero angularity in the centers. In addition to making intuitive sense, the concept of counter-rotating vortices downstream of an elbow has been reported numerous times in the technical literature. The measured angles failed to show these vortices nor do they diminish over the length of the duct. It was suggested that the angle measurements be repeated to confirm or disprove their validity.

Summary

Hot flue gas flow fields inside the breeching ductwork at Ohio Edison's Edgewater Station have been numerically modeled using a CFD package known as **VISCOUS**. Using test data supplied by Ohio Edison, comparisons were made between measured and predicted results. The simulated flow fields were shown to agree very well with pitot-tube-based velocity measurements. However, the study raised questions concerning the validity of the 3-D pitot tube angularity measurements.

The modeling technique was used to simulate the output from generic flow monitors. It was also shown that CFD can model flow control devices prior to installation to determine their effect and to aid in the restoration of uniform flow.

ACKNOWLEDGMENTS

Airflow Sciences Corporation would like to thank the following individuals for their support and contributions to the work contained in this report:

- **Electric Power Research Institute (EPRI)**
  - Charles E. Dene (Manager, SO_2 Control Projects)
  - Ellen M. Petrill (Manager, Plant Performance)
- **Fossil Energy Research Corp. (FERCo)**
  - Tom Martz
  - Lawrence J. Muzio, Ph.D.
- **Ohio Edison Company**
  - Adrian J. Cook (Environmental Specialist)
  - Dale Alan Kanary (Chemical Engineer)
- **Systems Applications International (SAI)**
  - Richard D. McRanie (Director, Utility Services)